

Metallomics

Integrated biometal science

Accepted Manuscript

This article can be cited before page numbers have been issued, to do this please use: S. Masuri, E. cadoni, M. G. Cabiddu, F. Isaia, M. G. Demuru, L. Morá, D. Bucek, P. Vanhara, J. havel and T. Pivetta, *Metallomics*, 2020, DOI: 10.1039/D0MT00006J.



This is an Accepted Manuscript, which has been through the Royal Society of Chemistry peer review process and has been accepted for publication.

Accepted Manuscripts are published online shortly after acceptance, before technical editing, formatting and proof reading. Using this free service, authors can make their results available to the community, in citable form, before we publish the edited article. We will replace this Accepted Manuscript with the edited and formatted Advance Article as soon as it is available.

You can find more information about Accepted Manuscripts in the [Information for Authors](#).

Please note that technical editing may introduce minor changes to the text and/or graphics, which may alter content. The journal's standard [Terms & Conditions](#) and the [Ethical guidelines](#) still apply. In no event shall the Royal Society of Chemistry be held responsible for any errors or omissions in this Accepted Manuscript or any consequences arising from the use of any information it contains.

Significance to Metallomics

View Article Online
DOI: 10.1039/D0MT00006J

Copper compounds, alone or in combination with other drugs, are promising anticancer agents. In a test on cancer cells treated with combinations of the ER stress antioxidative agent salubrinal and Cu(phen)₂(H₂O)(ClO₄)₂, we observed a modulatory effect that pushed us to verify a possible chemical interaction between the two molecules. A new compound was hypothesized and prepared showing that the introduction of the antioxidant salubrinal in the [Cu(phen)₂] core lead to a new molecule with high free radical scavenging activity and able to attenuate *in vitro* lipid peroxidation. The new compound was tested on A2780 and SKOV3 cells and the results may be exploited to enlarge the therapeutical portfolio of metal complexes as antitumoral drugs. This research is a cross-disciplinary study involving metallobiochemistry, pharmacology, medicine, and toxicology, and can provide a better understanding of the mechanisms of action of potential copper anticancer drugs, giving useful insights for the design of new active species.

Metallomics Accepted Manuscript

PAPER

The first copper (II) complex with 1,10-phenanthroline and Salubrinal with interesting biochemical properties

Received 00th January 20xx,
Accepted 00th January 20xx

DOI: 10.1039/x0xx00000x

Sebastiano Masuri,^a Enzo Cadoni,^a Maria Grazia Cabiddu,^a Francesco Isaia,^a Maria Giovanna Demuru,^a Lukáš Moráň,^{b,c} David Buček,^b Petr Vaňhara,^{b,c} Josef Havel,^{c,d} Tiziana Pivetta,^{*a}

The novel copper complex $[\text{Cu}(\text{phen})_2(\text{salubrinal})](\text{ClO}_4)_2$ (**COSAL**) has been synthesised and characterised. Copper(II) is coordinated by salubrinal through the thionic group, as shown by the UV-Vis, IR, ESI-MS and tandem mass results, together with the theoretical calculations. The formed complex showed a DPPH radical scavenging ability higher than that of salubrinal alone. Studies on the lipid oxidation inhibition, showed that the **COSAL** concentration, required to inhibit the enzyme, was lower than that of salubrinal. The inhibition of the enzyme could take place via allosteric modulation, as suggested by docking calculations. **COSAL** showed a good cytotoxic activity on A2780 cells, 82 fold higher than the precursor salubrinal and 1.4 fold higher than $[\text{Cu}(\text{phen})_2(\text{H}_2\text{O})](\text{ClO}_4)_2$. Treatment with **COSAL** in SKOV3 ovarian cancer cells induced expression of GRP-78 and DDIT3 regulators of ER-stress response. The cytotoxic effect of **COSAL** was reverted in the presence of TUDCA, suggesting that **COSAL** induces the cell death through ER-stress. In A2780 cells treated with **COSAL** γ -H2AX was accumulated, suggesting that also DNA was involved.

Significance to Metallomics

Copper compounds, alone or in combination with other drugs, are promising anticancer agents. In a test on cancer cells treated with combinations of the ER stress antioxidative agent salubrinal and $\text{Cu}(\text{phen})_2(\text{H}_2\text{O})(\text{ClO}_4)_2$, we observed a modulatory effect that pushed us to verify a possible chemical interaction between the two molecules. A new compound was hypothesized and prepared showing that the introduction of the antioxidant salubrinal in the $[\text{Cu}(\text{phen})_2]$ core lead to a new molecule with high free radical scavenging activity and able to attenuate *in vitro* lipid peroxidation. The new compound was tested on A2780 and SKOV3 cells and the results may be exploited to enlarge the therapeutical portfolio of metal complexes as antitumoral drugs. This research is a cross-disciplinary study involving metallobiochemistry, pharmacology, medicine, and toxicology, and can provide a better understanding of the mechanisms of action of potential copper anticancer drugs, giving useful insights for the design of new active species.

Introduction

At present days cancer represents one of the main causes of death in industrialized society. With the term “cancer”, we refer to a wide range of diseases that share some common traits, such as the abnormal proliferation of cells resulting in the growth of tissue masses, known as tumours. Since the discovery of the cytotoxic activity of cisplatin, several metal complexes have been proposed as antitumor agents with good potential biological activity and less side effects. Copper(II) has attracted much attention because of its ubiquity as cofactor of several enzymes and proteins,¹ and, since copper complexes with 1,10-phenanthroline (phen) were able to cleave DNA acting as

chemical nucleases,² several complexes containing nitrogen donor ligands have been designed and evaluated as anticancer agents. Previous studies evidenced how copper(II)-phenanthroline based complexes and in particular $[\text{Cu}(\text{phen})_2(\text{H}_2\text{O})](\text{ClO}_4)_2$ (**CO**, Fig. 1), induce massive cell death both on solid than in haematological human tumour cells.^{3–8} The involved molecular mechanism has been partially unveiled in a recent study where it has been evidenced how these compounds induce the pro-apoptotic branch of Unfolded Protein Response (UPR).⁹ UPR is a coordinating adaptive program that responds to accumulation of incorrectly processed proteins in the endoplasmic reticulum (ER), a condition known as ER stress. The final cell response is dependent on a specific activity of individual pathways and can lead to adaptation or apoptosis, especially when ER stress is prolonged or severe. Many evidences indicate that ER stress is involved also in the pathogenesis of misfolded protein diseases and in the cytotoxicity of environmental pollutants and industrial chemicals.^{10,11}

Salubrinal (2E)-3-phenyl-N-[2,2,2-trichloro-1-[[[8-quinolinylamino]thioxomethyl]amino]ethyl] 2-propenamide, **SAL**, Fig. 1) was discovered in an attempt to identify novel

^a Dipartimento di Scienze Chimiche e Geologiche, Università degli Studi di Cagliari, Cittadella Universitaria, 09042 Monserrato CA – Italy. E-mail: tpivetta@unica.it;

^b Department of Histology and Embryology, Faculty of Medicine, Masaryk University, Brno, Czech Republic.

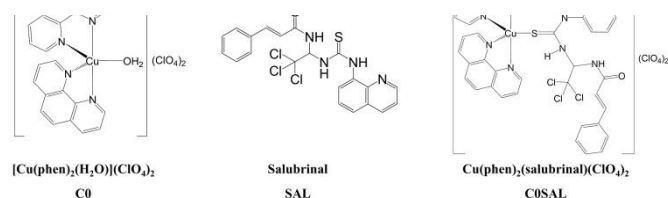
^c International Clinical Research Centre, St. Anne's University Hospital, Brno, Czech Republic.

^d Department of Chemistry, Faculty of Science, Masaryk University, Brno, Czech Republic.

*Electronic Supplementary Information (ESI) available. See DOI:10.1039/x0xx00000x

cytoprotective compounds that protect PC12 rat pheochromocytoma cells from ER stress-mediated apoptosis, induced by the N-glycosylation inhibitor Tunicamycin.¹² During UPR, dissociation of BiP (GRP 78) activates PERK (protein kinase RNA (PKR)-like ER kinase), an ER-resident transmembrane protein that phosphorylates eIF2 α (eukaryotic Initiation Factor 2, subunit α), in order to arrest protein synthesis under ER Stress. **SAL** proved to possess cytoprotective activity preventing eIF2 α dephosphorylation. Although the precise molecular mechanism has not been completely clarified yet, **SAL** is thought to interfere with the sequestration of eIF2 α by the protein complex GADD34-PP1 (Protein Phosphatase 1).^{12,13} Interestingly, studies of **CO** and variously substituted imidazolidine-2-thione³ complexes with general formula [Cu(phen)₂L](ClO₄)₂ revealed synergistic cytotoxic effect in combination with **SAL**. In particular, an enhanced upregulation in the expression of CHOP (DDIT3) as well as BiP (GRP78) was detected. From these results and considering that **SAL** has a backbone resembling the imidazolidine-2-thione structure, we deemed if **CO** and **SAL** were able to interact from a chemical point of view. The reactivity of the two molecules was studied and the formation of a complex between **CO** and **SAL**, named **COSAL** (Fig. 1), was observed. The coordination mode, the stability constant, the interaction with specific proteins, and the cytotoxic properties of the formed complex were studied. Moreover, the free radical scavenging activity as well as the *in vitro* inhibitory activity against soybean lipoxygenase of the new complex were measured and compared with that of the precursors **CO** and **SAL**. Combination studies with tauroursodeoxycholic acid (TUDCA) indicated the induction of ER-stress as the driving mechanism of cell death caused by **COSAL**.

Fig. 1 Molecular structures and acronyms of the studied compounds.



Material and methods

Reagents

Acetonitrile, methanol, isopropanol, dimethyl sulfoxide (DMSO), tetrahydrofuran (THF), acetone, absolute ethanol, sodium linoleate, lipoxygenase, butylated hydroxytoluene (BHT) and tris (hydroxymethyl) aminomethane hydrochloride (TRIS) were purchased from Merck (Milan, Italy). Toluene, potassium thiocyanate, copper(II) carbonate hydroxide and thionyl chloride were purchased from Alfa-Aesar. Trans-cinnamamide and chloral hydrate were purchased from TCI. 3-(4,5-dimethylthiazol-2-yl)-2,5-diphenyltetrazolium bromide (MTT) was purchased from Sigma-Aldrich (Czech Republic). The commercial reagents were used as received, without any

further purification. Ultrapure water was obtained with MilliQ Millipore. THF was distilled from sodium/benzophenone.

NMR

¹H NMR spectra were recorded on a Bruker Advance III HD 600 spectrometer at room temperature with tetramethylsilane (TMS) as internal standard in DMSO-d₆. Chemical shifts, multiplicity and coupling constants were reported.

Mass spectrometry studies

Mass spectra were recorded using a triple quadrupole QqQ Varian 310-MS mass spectrometer using the atmospheric-pressure ESI technique. The sample solutions were infused directly into the ESI source using a programmable syringe pump at a flow rate of 1.25 mL/h. A dwell time of 14 s was used, and the spectra were accumulated for at least 10 min in order to increase the signal-to-noise ratio. Mass spectra were recorded in the *m/z* 100 – 1200 range. The experimental conditions were: needle voltage 3500 V, shield 800 V, source temperature 60 °C, drying gas pressure 20 psi, nebulizing gas pressure 20 psi, detector voltage 1450 V. Tandem MS experiments were performed using argon as the collision gas (1.8 psi). The collision energy was varied from 5 to 40 V. The isotopic patterns of the measured peaks in the mass spectra were analysed using the mMass 5.5.0 software package.^{14,15} High resolution mass spectra were recorded on a Thermofisher ESI-MS/MS-ORBITRAP-ELITE and Velos PRO. The sample solutions were infused directly into the ESI source using a programmable syringe pump at a flow rate of 5 μ L/min. Mass spectra were recorded in the *m/z* 700 – 950 range. The experimental conditions were: needle voltage 2.5 kV, shield 0.8 kV, source temperature 50 °C, drying gas pressure 20 psi, nebulizing gas pressure 20 psi, detector voltage 1.3 kV.

Spectrophotometric studies

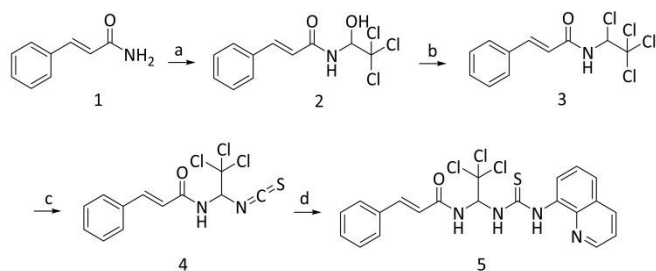
UV–Visible spectrophotometric measurements were performed in the range 200 – 1100 nm on an Agilent Cary 60 spectrophotometer, using a 1 cm quartz cell at 25 °C. The formation constant of the complex formed by **CO** with **SAL** was determined at 25 °C by spectrophotometric titration in acetonitrile solution in 0.05 M NaClO₄ ionic buffer. The number of linearly independent absorbing species was obtained by applying eigenvalues analysis on the absorbance data matrix. The complex formation constant, expressed as overall association constant, was calculated using the Hyperquad 2006 program.¹⁶ The stoichiometry of the formed complex was also studied by continue variation method (Job's plot).^{17,18} IR spectra were acquired with a Bruker Vector 22 spectrophotometer, preparing the samples as KBr pellets.

Synthesis of Salubrial (SAL)

SAL was synthesized according to a reported method¹⁹ with modifications required to increase the purity of the final product. Synthetic pathway is reported in **Scheme 1**.

In brief, toluene (136 mL) was added to the mixture of cinnamamide (**1**, 6.8 mmol) and chloral hydrate (6.8 mmol). The mixture was left under reflux for 4 h. After cooling, the white crystalline solid **2** was precipitated, filtrated and dried. The solid (**2**) was dissolved in dry THF (20 mL) and chlorinated by reflux with SOCl_2 (25.8 mmol) for 2 h. The yellow solid (**3**) was yielded by evaporating the solvent and washing with cold petroleum ether. By refluxing with potassium thiocyanate (8.4 mmol) in acetone (18 mL) for 2h, it was transformed to isothiocyanate (**4**). The titled compound was used as crude and refluxed in dry THF (8.4 mL) with quinolin-8-amine (4.2 mmol) for 2 h. After solvent evaporation the residue was washed with dichloromethane obtaining **5** as a white powder. The former one was then suspended and stirred in distilled water to dissolve the soluble thiocyanate. The white solid was recovered by filtration under vacuum and Fe (III) solution (1 mM) was added to the supernatant to check the formation of the red compound $[\text{Fe}(\text{SCN})_6]^{3+}$. The washing procedure was repeated until the supernatant solution stayed colourless upon the addition of the iron solution. The recovered solid was washed with ethyl ether and dried. Yield was 75 %.

(2E)-3-phenyl-N-[2,2,2-trichloro-1-[(8-quinolinylamino)thioxomethyl]amino]ethyl]-2-propenamide, SAL (5**):** Spectroscopic data were consistent with those reported in the literature.¹⁹ ESI-MS, m/z found: 479.3 (calc. 479.0), $[\text{M}+\text{H}]^+$, with the expected isotopic pattern. $^1\text{H-NMR}$ (Fig. S1) (600 MHz, DMSO-d_6 , δ , ppm): 11.03 (s, 1H), 9.58 (s, 1H), 9.04 (d, 2H, $J = 7.76$ Hz), 8.96 (dd, 1H, $J = 4.40$ Hz, $J = 1.28$ Hz), 8.43 (d, 1H, $J = 8.14$ Hz), 7.72 (d, 1H, $J = 7.02$ Hz), 7.66 (q, 1H, $J = 4.05$ Hz), 7.56-7.61 (m, 5H), 7.39-7.45 (m, 3H), 6.91 (d, 1H, $J = 15.70$ Hz). Elemental analysis: expected C 52.57, H 3.57, N 11.68, found C 52.53, H 3.61, N 11.70.



Scheme 1. Reagents and conditions: (a) chloral hydrate, toluene, rf 4h; (b) SOCl_2 , dry THF, rf 2h; (c) KSCN, acetone, rf 2h; (d) quinolin-8-amine, dry THF, rf 2h.

Synthesis of Cu(II)-phenantroline complexes

CO: The precursor $[\text{Cu}(\text{phen})_2(\text{OH})_2](\text{ClO}_4)_2$ (**CO**) was prepared as previously described.³ In brief, perchloric acid was added to an ethanolic suspension of $\text{Cu}_2(\text{CO}_3)(\text{OH})_2$, the resulting solution was cooled and an ethanolic solution of 1,10-phenanthroline (1:2 Cu:phen molar ratio) was added, the formed blue-green precipitate was filtered off, washed with ethanol and dried at room temperature (Yield 85 %). **COSAL:** $[\text{Cu}(\text{phen})_2(\text{SAL})](\text{ClO}_4)_2$

was prepared as following: **SAL** (white in colour, 0.067 mmol) was suspended in 4.0 mL of 2-propanol and slowly added to a suspension of **CO** (blue in color, 1 eq) in 4.0 mL of 2-propanol. The reaction mixture was stirred at room temperature for 24 hours, since a green powder was obtained. The desired product (**COSAL**, 0.0490 g) was recovered by filtration in vacuum, washed with diethyl ether and dried. Yield was 66 %. Elemental analysis: expected C 49.02, H 3.02, N 10.16, found C 49.12, H 3.00, N 10.12. ESI-MS. m/z , found (calc.): 1000.0 (1000.0) $[\text{Cu}(\text{phen})_2(\text{SAL})(\text{ClO}_4)]^+$, with the expected isotopic pattern. FT-IR (KBr), cm^{-1} : 1661 (C=O). UV-Vis (CH_3CN , NaClO_4 0.05 M) $\log \epsilon$ (λ , nm): 5.22 (268), 3.82 (289, sh).

Determination of the reducing activity of the stable radical 1,1-diphenyl-picrylhydrazyl (DPPH)

Each test compound was dissolved in DMSO at 1.0 mM concentration, then a 1:10 dilution was performed with absolute ethanol. DPPH solution (0.1 mM, absolute ethanol) was prepared freshly, stored in the dark and used in a few hours. The test solution (1500 μL) was added to an equal volume of DPPH inside the cuvette and the absorbance in the range 200 - 650 nm was recorded at room temperature for 70 minutes. The absorbance at 517 nm was evaluated to examine the time-dependence of the radical scavenging activity (RA).^{20,21} RA of each compound was expressed as the percentage inhibition of the absorbance of the initial DPPH solution (RA %). BHT (butylated hydroxytoluene) was used as reference compound.

Soybean lipoxygenase inhibition study in vitro

Stock solution of **CO**, **SAL** and **COSAL** were dissolved in DMSO at ≈ 0.1 mM concentration, then the proper dilution was performed with TRIS buffer at pH 7.4. Sodium linoleate (0.00200 g, V 10.0 mL, ≈ 0.65 mM) and soybean lipoxygenase (0.00200 g, V 10.0 mL, $\approx 2 \times 10^{-6}$ M) were dissolved in TRIS buffer at pH 7.4, and the required dilutions were performed with TRIS buffer at pH 7.4. Solutions of sodium linoleate, soybean lipoxygenase and **SAL** were prepared daily and kept in the dark at 5°C. The conversion of sodium linoleate to 13-hydroperoxylinoleic acid was monitored recording the absorbance at 243 nm. The absorbance at 243 nm and not at 234 nm (maximum) was chosen since at 234 nm the contribution of **CO** or **COSAL** absorbance was too relevant.

DFT calculations

Geometry optimization of **SAL** and the copper complexes $[\text{Cu}(\text{phen})_2(\text{H}_2\text{O})]^{2+}$ and $[\text{Cu}(\text{phen})_2(\text{SAL})]^{2+}$ were performed on an Intel-i7 based system using the release 4.2 of ORCA.²² Input files for DFT calculations were prepared using Avogadro 1.2.0.²³ Geometry optimizations were performed at DFT level, using the hybrid PBE0 functional²⁴ and def-2 TZVP basis set.²⁵ The molecular geometry optimizations were performed starting from structural data, when available. IR frequency calculations were carried out to verify the nature of the minima of each optimization by assessing the absence of calculated negative

frequencies. Atomic charges at natural population analysis (NPA) level were calculated by means of JANPA software package.²⁶ Molecular orbital shapes and energies were investigated using Chemcraft v1.8.²⁷

Docking calculations

Molecular docking calculations were performed using Autodock Vina software.²⁸ DFT optimized ligands and Cu (II) complexes were exported as PDB files. X-Ray structure of the complex between soybean lipoxygenase LOX-3 and 3,4-dihydroxybenzoic acid (PDB:1N8Q) was chosen as receptor.²⁹ Prior to docking, both ligands and receptor were processed using MG Labs Autodock Tools.³⁰ In the receptor crystal, water molecules and 3,4-dihydroxybenzoic acid (dhb) were removed, while polar hydrogens and Gasteiger charges were added. Atomic charge for Fe2858 cofactor was manually adjusted in the generated pdbqt file. For all the ligands, polar hydrogens and Gasteiger charges were added, while no rotational constraints were applied. Atomic charges for copper were manually adjusted in the generated pdbqt files. Validation of the docking protocol was performed by docking ligand dhb into its binding pocket. A grid cube of 20×20×20 points centred at coordinates $x = 21.287$, $y = 1.743$, $z = 19.171$ with a spacing of 1.0 Å, was chosen for this purpose. All the tested compounds were docked as competitive inhibitors or allosteric modulators. In the first case, docking calculations were performed using the parameters reported above. In the second case, a grid box of 30×25×20 points centred at coordinates $x = 24.970$, $y = 11.444$, $z = -0.396$ with a spacing of 1.0 Å, was chosen. Molecular interactions and docked poses were evaluated using Biovia Discovery Studio Viewer v19 (free version).³¹

Viability assay

Cells were cultured for 24 h on a 96-well plate at a density of 10 000 cells per well in medium containing **CO** and **SAL** either alone or in combination, or **COSAL**, at the indicated concentrations. The respective solvents were used as controls. Then, the MTT reagent was added directly to the culture medium for 4 h. Medium, including MTT reagent, was aspirated and the cells lysed by addition of 90 % isopropanol, 0.04 M HCl and 10 % Triton/Tween. Absorbance was recorded at 570 nm by a Synergy HTX multi-mode reader (BioTek Instruments, VT, USA). All the measurements were performed in technical pentaplicates and repeated in three independent experiments.

Transmission electron microscopy (TEM)

Cells treated by **SAL** were harvested using trypsin-EDTA, washed with PBS, fixed in 3 % glutaraldehyde with 0.2 % tannin in 0.1 M cacodylate buffer for 1 hour, and postfixed in 1 % OsO₄ in the same buffer for 50 min. After post-fixation, cells were washed three times with cacodylate buffer and embedded in small blocks of 1 % agar, 1 mm³ in size. Agar blocks were dehydrated in increasing concentrations of ethanol (50 %, 70 %, 96 %, and 100 %), treated 2 x 10 min with 100 % acetone, and embedded in Durcupan resin. Ultrathin sections were prepared

on Leica EM UC6 ultramicrotome, stained with uranyl acetate and Reynold's lead citrate, and examined with the FEI Morgagni 286(D) TEM. One hundred cells from each experimental group was examined. Cytological analysis of TEM images was performed by two independent reviewers (PV, LM).

Immunofluorescence measurements

Cells were washed three times in 1 × PBS (pH 7.4), fixed in 4% paraformaldehyde for 15 min at room temperature, washed with 1 × PBS containing 3% BSA and 0.1% Triton X-100 and incubated with DDIT3 (#2895) or GRP-78 (#3177) antibodies (both from Cell Signaling, MA, USA), diluted 1 : 200 at 4°C overnight. Immunofluorescent signals were obtained by Alexa Fluor conjugated secondary antibodies (AF488, cat. no. A32731 or AF568, cat. no. A11004, both from Life Technologies, USA), diluted 1 : 2000. Cell nuclei were visualized by DAPI (Life Technologies, USA). Immunofluorescence was recorded using Zeiss Axio Observer Z1 microscope equipped with a LSM800 confocal unit.

SDS-PAGE and western blotting

Trypsinised cells were washed two times with ice-cold 1× PBS and resuspended in NP-40 lysis buffer containing 50 mM Tris-Cl (pH 7.4), 150 mM NaCl, 2 mM EDTA, 1% NP-40, 50 mM NaF supplemented with phosphatase inhibitor cocktail (PhosStop, Roche Applied Science, Czech Republic) and protease inhibitor cocktail (complete, Roche Applied Science, Czech Republic). Protein content in the cell extract was quantified using the Bradford-based BioRad protein Assay Kit (BioRad). Cell extracts were then mixed with 2x Laemmli sample buffer (100 mM Tris pH 6.8, 4% SDS, 200 mM DTT, 20% glycerol, and 0.1% bromophenol blue) and boiled for 3 min. An equivalent of 15 mg proteins was resolved using 10% sodium dodecylsulfatepolyacrylamide gel electrophoresis (SDS-PAGE). Resolved proteins were then electroblotted onto a 0.45 mm polyvinylidene difluoride (PVDF) membrane (Millipore, Czech Republic) and incubated with the indicated primary antibodies diluted 1 : 200–1 : 1000 at 4 °C overnight (Actin, cat. no: CST13E5 from Cell Signaling, MA, USA, and γ -H2AX, cat. no: ab81299 from Abcam, UK). Blots were developed using horseradish peroxidase (HRP)-conjugated anti-rabbit HRP #7074 (Cell Signaling, USA) secondary antibody, diluted 1 : 5000, and Immobilon Western HRP Substrate (Millipore, Czech Republic), according to the manufacturer's protocols.

Results and discussion

Synthesis

Salubrinol: SAL was initially synthesized according to the reported method¹⁹, however unreacted thiocyanate was evidenced in the IR spectrum of the obtained product (see supplementary, Fig. S2). This issue was observed also changing reaction conditions such as time and thiocyanate amount. The washing procedure reported in the experimental section

allowed the complete removal of the former impurity, as confirmed by IR spectroscopy (Fig. S3B). **SAL** is soluble in DMSO and CH₃CN up to 10⁻¹ M and 4.0 mM concentrations respectively. **SAL** could be also solubilized in CH₃CN:H₂O (1:1 mixture) up to 0.5 mM level. Solubility of **SAL** in H₂O and TRIS might be enhanced by dissolving the titled compound in DMSO prior to dilution. In this case, sonication and vigorous mixing should be avoided in order to prevent the formation of emulsions. **SAL** solutions prepared in pure DMSO or CH₃CN are stable at rt for 48 hours, while DMSO:H₂O and DMSO:TRIS solutions are stable at rt up to 6 hours. A change of the solutions appearance (from colourless to yellow) and the development of sulphurous smell were observed for longer storage periods.

COSAL copper complex: by reaction between **C0** and **SAL** in the proper molar ratio, the novel complex [Cu(phen)₂(SAL)](ClO₄)₂ (**COSAL**) was obtained by substitution of the water with a **SAL** molecule into the metal core. The stoichiometry of the novel complex has been proposed on the basis of elemental analysis (see experimental), Job's plot (see section Spectrophotometric studies) and ESI-MS spectrometry. In the ESI-MS spectrum of [Cu(phen)₂(SAL)](ClO₄)₂ (Fig. 2A) a peak at 1000 *m/z* due to the [Cu(phen)₂(SAL)(ClO₄)]⁺ species was observed, as a charged fragment of the neutral precursor [Cu(phen)₂(SAL)](ClO₄)₂. In addition, a peak at 450.5 *m/z* due to the doubly charged ion [Cu(phen)₂(SAL)]²⁺ was highlighted. Several fragments containing the deprotonated **SAL**, originated in ESI phase by loss of HClO₄, together with Cu(I) complexes, were observed in the mass spectrum (the reduction of Cu(II) to Cu(I) is widely observed in ESI phase, depending on the solvent³²). The identity of the reported ions was confirmed by matching between calculated and experimental isotopic patterns (Fig. S4) and tandem mass experiments (see Mass spectrometry). The mass spectrum was also recorded at high resolution in the 700-950

m/z range (Fig. 2B), to determine the exact masses for the peaks at 720 and 900 *m/z* and confirm the proposed chemical formula. As can be seen in Fig. 2C, the fitting of the isotopic pattern and the matching of the experimental exact masses with those calculated (720.0096 u versus 720.0094 u and 900.0776 u versus 900.0781 u), confirm the proposed stoichiometry. The formed copper complex is stable in the solid state at room temperature, without particular precautions. It is soluble in DMSO at 0.1 M concentration level, in CH₃CN at 0.01 M, and in H₂O:CH₃CN mixture (1:1) at 0.1 mM. Solubility in water and ethanol might be enhanced by dissolving the titled compound in DMSO at 1.0 mM prior to dilution at the desired concentrations. **COSAL** is also soluble in TRIS buffer by dissolving it in DMSO at 0.1 mM prior to dilution. In this case, sonication or vigorous mixing should be avoided while performing dilutions, in order to prevent the formation of emulsions. Stock solutions of **COSAL** in DMSO and CH₃CN are stable at 4°C up to 6 months. Stock solutions in H₂O:CH₃CN, DMSO:H₂O, DMSO:EtOH and DMSO:TRIS could be stored at rt for 48hrs., but should be prepared daily and stored in the darkness for enzymatic and antioxidant assays. The absorption spectra of **COSAL** in DMSO:TRIS (0.5:99.5) after 0 and 48 hrs. are shown in the Supporting (Fig. S21). In order to check the stability of **COSAL** in a medium similar to the aqueous one, the former compound was dissolved in H₂O:CH₃CN (1:1) mixture at 25 μM concentration and spectral variation in the range 200-400 nm were followed for 24 hrs. by recording 1 spectrum every 60 minutes (Fig S5A). No significant variations were observed at both maxima levels (225 and 269 nm respectively).

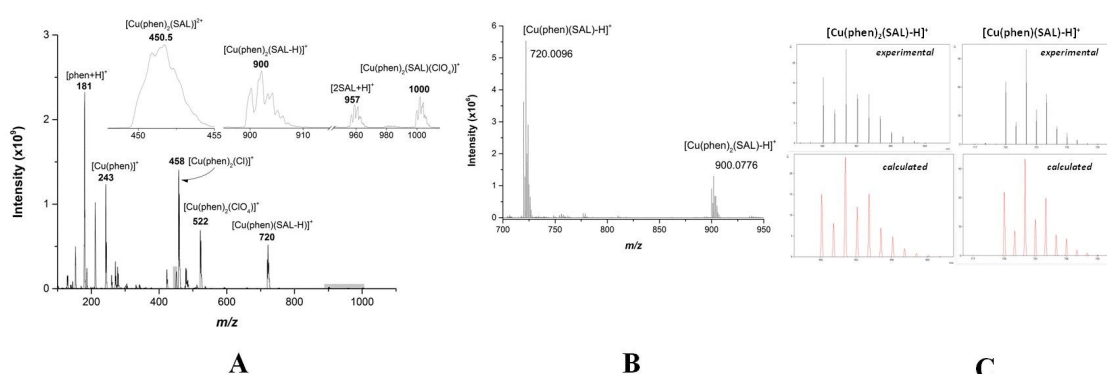


Fig. 2 (A) ESI-MS spectrum of **COSAL** [Cu(phen)₂(SAL)](ClO₄)₂, (B) high resolution mass spectrum in the 700-950 *m/z* range, (C) experimental and calculated isotopic pattern for peaks at 700 and 900 *m/z*. (isopropanol:methanol:water 2:1:1).

Spectrophotometric studies

To determine the number and the stoichiometry of the complex formed between **C0** and **SAL**, the method of continuous variation (Job's method) was applied.^{17,18} Absorption spectra were collected varying from 0 to 1 the ligand molar fraction (Fig. S6A). Absorbance data at 966 and 722 nm, corrected for the

absorbance of the pure reactants, reported as a function of the ligand molar fraction (Fig. S6B), clearly indicates a 1:1 ($\chi_L = 0.5$) ligand to metal complex. Once defined the complexation model, the complex formation constant was determined by spectrophotometric titration. Equilibrium studies of **C0** and **SAL** were carried out in acetonitrile in the 200 – 400 nm range. In

Fig. S7 selected spectra recorded during the titration of **SAL** with **CO** and of **CO** with **SAL** are reported as an example. By adding increasing amounts of **SAL** (Fig. S7A) or **CO** (Fig. S7B), new absorption bands were evidenced, a feature consistent with an interaction altering the solvated cationic core. Isosbestic points appeared during the titration, providing evidence for at least one equilibrium. From eigenvalue analysis of the spectrophotometric data, three significant eigenvalues were found, indicating three linearly independent absorbing species in solution. By fitting the experimental data considering the species $[\text{Cu}(\text{phen})_2]^{2+}$, **SAL** and $[\text{Cu}(\text{phen})_2(\text{SAL})]^{2+}$, the complex formation constant expressed as $\log \beta$ was determined (5.10 ± 0.07). As can be seen in Fig. S7, the spectral variations are different in the two titrations, but in both the cases they are in agreement with a 1:1 model, i.e. with the formation of the complex $[\text{Cu}(\text{phen})_2(\text{SAL})]^{2+}$.

Coordination mode in **COSAL**

Since any attempt to obtain single crystals suitable for X-rays analysis was unsuccessful, coordination mode around the metal ion for the novel **COSAL** complex was proposed by combining the experimental data, UV-Vis, IR, ESI-MS and tandem MS spectrometry, with the theoretical calculations.

UV-Vis. UV-Vis spectrum of **COSAL** in the region between 400 - 1100 nm (Fig. S5B) features a maximum at 714 nm and a shoulder at 914 nm. A penta-coordinated geometry might be proposed also for **COSAL**, in agreement with the absorption spectra of variously substituted $[\text{Cu}(\text{phen})_2(\text{imidazolidine-2-thione})](\text{ClO}_4)_2$ complexes.³ See for comparison the UV-Vis spectrum of **CO** (Fig. S6A, black line), where two wide bands with similar heights are present, typical of an octahedral coordination mode around the copper ion³³ (in this case, the sixth position around the metal centre is occupied by a solvent molecule³⁴).

IR. From comparison of the IR spectra of **COSAL** (Fig. S3C) with the parent compounds **CO** (Fig. S3A) and **SAL** (Fig. S3B), a coordination of the **SAL** carbonyl oxygen to the metal centre might be excluded, since there is no significative shift in its stretching signal (1660 cm^{-1}) upon complexation. Univocal attribution of thiocarbonyl, amidic and thioamidic NH groups of **SAL**, already difficult by the overlapping of skeletal backbone frequencies, becomes more complicated in **COSAL** by the concomitant presence of the phen signals ($1000 - 500 \text{ cm}^{-1}$). The wide peak at 1100 cm^{-1} , present in **CO** and **COSAL**, is due to the perchlorate anions.

Mass spectrometry. Tandem MS experiments at different collision energies (CE) were performed to define the identity of all the peaks relative to species containing copper, phenanthroline and **SAL** and to finally hypothesise the structure of the parent compound **COSAL**. Since **SAL** has several coordinating atoms, all the possible resulting structures for **COSAL** were considered, however only one could explain the

fragmentation pathways observed during the tandem mass experiments. As regards the bi-charged ion $[\text{Cu}(\text{phen})_2(\text{SAL})]^{2+}$ (m/z 450.5), at CE 5.0 V two fragments were originated, at 181 m/z ($[\text{phen} + \text{H}]^+$) and 720 m/z ($[\text{Cu}(\text{phen})(\text{SAL-H})]^+$) (Fig. 3), and this fragmentation process might occur under the pathway depicted in Fig. S8A: i.e. the amidic proton on the **SAL** moiety is transferred to one phen molecule with subsequent nucleophilic attack by the deprotonated nitrogen to the metal centre. The proposed coordination mode for the 720 m/z fragment, is well reasonable since *i)* the amidic proton of **SAL** moiety is more acidic than the thioamidic ones and more prone to be transferred to one of the phen molecules, *ii)* the former deprotonation brings to a stable 6-membered metal chelated ring (a comparable mechanism was previously proposed for similar copper-phenanthroline complexes⁶). As can be observed in Fig. 3, as CE increased, a gradual decrease in intensity of the peak at 720 m/z is observed, until its complete disappearance at CE = 20 V. In contrast, an increase in intensity for peaks at 276 m/z $[\text{Cu}(\text{phen})(\text{SH})]^+$ and 243 m/z $[\text{Cu}(\text{phen})]^+$ is observed. This behaviour is consistent with an additional fragmentation of the ion with 720 m/z . Proposed fragmentation patterns are reported in the Supplementary (Fig. S8B-C). Tandem MS fragmentation of 720 m/z ($[\text{Cu}(\text{phen})(\text{SAL-H})]^+$) and 900 m/z ($[\text{Cu}(\text{phen})_2(\text{SAL-H})]^+$) (Fig. S9) follow a similar pattern. In particular, 900 m/z is generated as rearrangement product in ESI phase, while 720 m/z comes both from 900 m/z by loss of

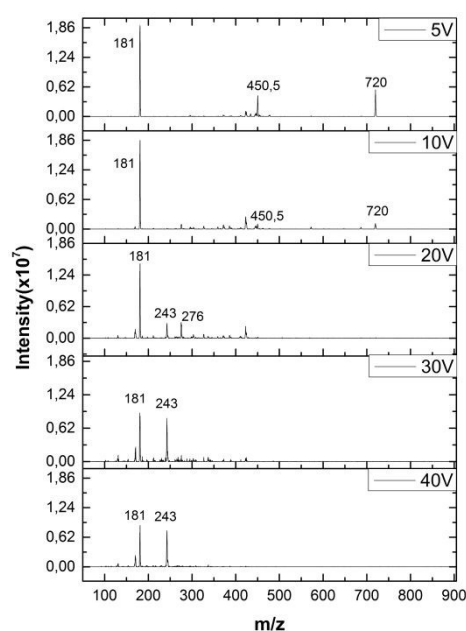


Fig. 3 Tandem MS fragmentations at different collision energies of the peak at 450.5 m/z ($[\text{Cu}(\text{phen})_2(\text{SAL})]^{2+}$). All the mass values are indicated as monoisotopic masses, computed as the sum of the masses of the primary isotope of each atom in the molecule (note that the monoisotopic mass may differ from the nominal molecular mass, in particular for big molecule). one phen unit (Fig. S10A) and by 450.5 m/z as previously shown. Both of them, share common product ions, e.g. 276, 243 m/z whose fragmentation mechanism was previously explained, while formation of 386 m/z might be hypothesized by the

migration process shown in Fig. S10B. As regards $[\text{Cu}(\text{phen})_2(\text{SAL})(\text{ClO}_4)]^+$ (m/z 1000), the main product peak at $522\ m/z$ ($[\text{Cu}(\text{phen})_2(\text{ClO}_4)]^+$) is due to the loss of a neutral **SAL** molecule. A further loss of a phen unit with generation of peak at $342\ m/z$ ($[\text{Cu}(\text{phen})(\text{ClO}_4)]^+$) can be observed at high voltage (Fig S11). The absence of ions containing **SAL** fragments bonded to $[\text{Cu}(\text{phen})_x]^+$ could be attributed to the steric hindrance of **SAL** itself and supports, in accordance with the findings previously reported, a coordination of **SAL** by a neutral donor group. Considering the strong affinity of copper for sulphur donating groups, and in accordance with molecular structures of similar mixed Cu(II)-phenanthroline complexes with thioamides^{3,35}, a pentacoordinated geometry around copper ion and a coordination of **SAL** via sulphur atom are proposed for $[\text{Cu}(\text{phen})_2(\text{SAL})](\text{ClO}_4)_2$. More insights about them are provided by DFT calculations.

DFT calculations. In order to assess the performance of the DFT protocol employed in this work, theoretical calculations were initially performed on the parent copper complex $[\text{Cu}(\text{phen})_2(\text{H}_2\text{O})]^{2+}$, starting from the **CO** X-ray structural data.³⁶ DFT optimized structure of $[\text{Cu}(\text{phen})_2(\text{H}_2\text{O})]^{2+}$ is reported in Fig. 4A. As can be seen, a trigonal bipyramidal geometry was predicted in analogy with the experimental data. In Fig. S12 the superimposition of DFT-optimized and experimental structures is reported (root mean square deviation was 0.0905 Å). In Table S1, selected bond lengths, angles and dihedrals for both X-Ray and DFT structures are reported. A very good linear correlation between experimental and theoretical parameters was obtained (Fig. S13), especially if we consider that the experimental data are relative to the solid state, while the DFT ones are calculated in gas phase. Atomic charges, computed at NPA level (Table S2), show on copper ion a significant lower

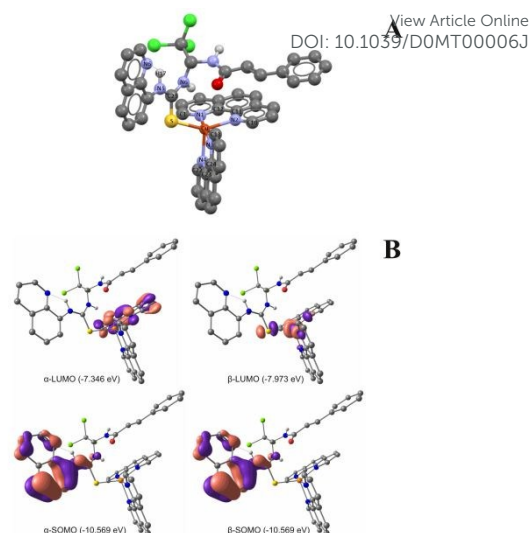


Fig. 4 Molecular drawings and atom labelling schemes for $[\text{Cu}(\text{phen})_2(\text{SAL})]^{2+}$ (A) at the DFT-optimized geometry. Isosurface drawings of selected frontier molecular orbitals calculated for (B) $[\text{Cu}(\text{phen})_2(\text{SAL})]^{2+}$ (contour value: 0.05). Non-polar hydrogen atoms are omitted for clarity.

occupied frontier MOs shows the highest Singly Occupied Molecular Orbital (SOMO) centred on the phenanthroline ligands, while the Lowest Unoccupied Molecular Orbital (LUMO) centred mainly on the metal ion (Fig. 4C). DFT optimized geometry for both **SAL** and $[\text{Cu}(\text{phen})_2(\text{SAL})]^{2+}$ were obtained using the same computational setup for $[\text{Cu}(\text{phen})_2(\text{H}_2\text{O})]^{2+}$. In case of **SAL** (Fig. 4B), the optimized geometry is stabilized by an intramolecular hydrogen bond between H10 and O forming a pseudo oxadiazine ring with H10...O length of 1.94 Å and H10...OC9 angle of 102.37 Å. In Table S3 selected bond lengths, angles and dihedrals are reported. An analysis of the frontier molecular orbitals (Fig. 4D) reveals both HOMO-1 and HOMO highly centred on the sulphur thioamide moiety, supporting the hypothesis of a coordinating ability through this donor group. DFT optimized structure of $[\text{Cu}(\text{phen})_2(\text{SAL})]^{2+}$ (Fig. 5A) shows an intermediate geometry between trigonal bipyramidal and square pyramidal, as evidenced by the value of the geometrical parameter $\tau = \frac{\beta - \alpha}{60}$ of 0.42.³⁷ As expected, a tetragonal distortion due to Jahn-Teller effect is observed, with the elongation of basal bond lengths (e.g. S-Cu, N2-Cu and N4-Cu equals to 2.379, 2.184 and 2.108 Å respectively) accompanied by the shortening of the axial ones (e.g. N1-Cu and N3-Cu equals to 2.014 and 2.037 Å respectively). A comparison between C-S bond lengths in **SAL** and in $[\text{Cu}(\text{phen})_2(\text{SAL})]^{2+}$ shows a significant reduction of the double bond character (1.661 and 1.712 Å, respectively), in agreement with similar systems structurally characterized.³ The DFT optimized geometry of $[\text{Cu}(\text{phen})_2(\text{SAL})]^{2+}$ is further stabilized by an intramolecular hydrogen bond between H17 and N6 (1.907 Å). Selected values of calculated bond lengths, angles and dihedrals are reported in Table S4. As observed for $[\text{Cu}(\text{phen})_2(\text{H}_2\text{O})]^{2+}$, both atomic charges (Table S5) and frontier molecular orbitals (Fig. 5B) suggest a LMCT behaviour.

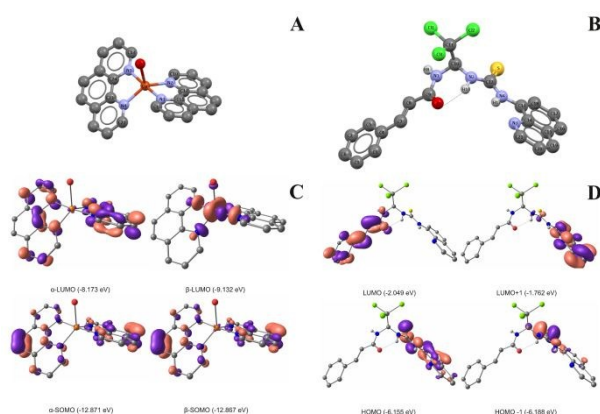


Fig. 5 Molecular drawings and atom labelling schemes for $[\text{Cu}(\text{phen})_2(\text{H}_2\text{O})]^{2+}$ (A) and **SAL** (B) at the DFT optimized geometry. Isosurface drawings of selected frontier molecular orbitals calculated for (C) $[\text{Cu}(\text{phen})_2(\text{H}_2\text{O})]^{2+}$ and (D) **SAL** (contour value: 0.05). Hydrogen atoms (A,C) and Non-polar hydrogen atoms (B,D) are omitted for clarity.

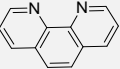
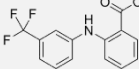
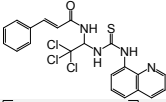
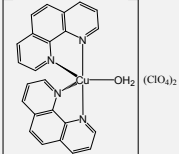
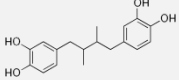
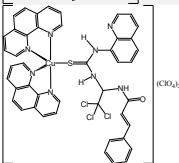
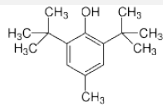
atomic charge if compared with its formal charge +2, suggesting a Ligand to Metal Charge Transfer (LMCT). The former trend is observable both at molecular orbital level: an analysis of beta

Determination of the reducing activity of the stable radical 1,1-diphenyl-picrylhydrazyl (DPPH)

Molecules that exhibit DPPH radical scavenging ability might show also anticancer and anti-inflammatory activities, and, under this light, the model of the scavenging of the stable DPPH radical is widely exploited to evaluate the antioxidant activity of promising compounds. DPPH may accept a radical hydrogen to be converted in a diamagnetic form, whose absorption spectrum differs from the previous one. The DPPH radical has a deep violet colour in solution ($\lambda_{\text{max}} = 530 \text{ nm}$), while the diamagnetic form is pale yellow coloured.³⁸ Following the change in the optical absorption at 520 nm it is possible to monitor the course of the reaction during the time and compare the scavenger ability of different compounds. Results on DPPH radical scavenging ability measured for **C0**, **SAL** and **COSAL** are reported in the Supplementary (Fig. S14). **C0** did not show any reducing activity in 60 min, as expected since the copper complex does not have any hydrogen to be lost as H^\bullet , and the

1,10-phenanthroline does not show reducing activity (6 % at 20 min, 8 % at 60 min³⁹). **SAL**, having three hydrogen atoms to be involved in the redox reaction, exhibited an interesting reducing activity, that is of $\approx 80 \%$ after 20 min and almost quantitative ($\text{RA} \approx 100 \%$) after 50 min. This reduction process is even faster than that of BHT (31 % at 20 min, 60 % at 60 min²⁰). As regards **COSAL**, this mixed complex not only exhibited a reducing activity, but this was almost 100 % completed after 3 min, showing that the coordination with the $\text{Cu}(\text{phen})_2$ backbone increases the reducing activity of the **SAL** of the 260 % at 3 min. It is interesting compare the % of RA shown by other copper complexes containing nitrogen donor chelator and an auxiliary ligand similar to **SAL**. In Table 1 are reported the % of RA for some complexes and the related auxiliary ligand. As can be seen, the novel complex **COSAL** presents the highest radical scavenging ability.

Table 1 Interaction percentage with DPPH (RA %) shown by ligands and copper complexes; phen is 1,10-phenanthroline, bipy is 1,10-bipyridine, fluf is deprotonated flufenamic acid (N-(α,α,α -Trifluoro-m-tolyl)anthranilic acid), NDGA is norhydroguaiaretic acid, BHT is butylated hydroxytoluene (0.05 mM EtOH, 25°C).

Compound	RA% at 20'	RA% at 60'	Structure	Ref.	Compound	RA% at 20'	RA% at 60'	Structure	Ref.
phen	< 1	< 1		this work, ³⁹	Hfluf	7.36	9.74		20
Salubrinol SAL	82.0	97.0		this work	$\text{Cu}(\text{fluf})(\text{bipy})\text{Cl}$	9.48	10.01		20
$\text{Cu}(\text{phen})_2(\text{OH}_2)(\text{ClO}_4)_2$ C0	2.1	4.0		this work	NDGA	81.02	82.60		20
$\text{Cu}(\text{phen})_2(\text{SAL})(\text{ClO}_4)_2$ COSAL	96.5	97.0		this work	BHT	31.30	60.00		20
$\text{Cu}(\text{fluf})(\text{phen})\text{Cl}$	22.46	26.52		20					

Soybean lipoxygenase inhibition study in vitro

Several experiments were performed keeping constant the concentration of substrate and enzyme and varying that of **C0**, or **SAL**, or **COSAL**, obtaining the following results:

- in the absence of **C0**, the conversion of sodium linoleate to 13-hydroperoxylinoic acid is completed in approx. 20 – 30 min, while in the presence of **C0**, the rate of the reaction is lowered (20 – 40 min), and the conversion percentage never raises the 100 % (Fig. S15A);

- ii) in the presence of increasing amounts of **SAL**, the absorbance decreases with the time with a trend similar for all the curves. The conversion of sodium linoleate to 13-hydroperoxylinoleic acid ends in approx. 40 - 60 min in the presence of **SAL** and the conversion percentage never raises the 100 % (Fig. S15B);
- iii) in the presence of increasing amount of **COSAL**, the absorbance decreases with the time with a trend similar for all the curves. The conversion of sodium linoleate to 13-hydroperoxylinoleic acid ends in approx. 60 - 80 min in the presence of **COSAL** and the conversion percentage never raises the 100 % (Fig. S15C);

Reporting the inhibition percentage (IP) as a function of the inhibitor concentration (Fig. 6), it was found that IP varies with time for every given concentration. This trend became invariant after 30 min for **CO**, 20 min for **SAL** and 5 min for **COSAL**. This time was chosen as the reference one to calculate the IC_{50} , i.e. the concentration required to inhibit the 50 % of the enzyme. For the three compounds, IC_{50} resulted to be $55 \pm 5 \mu\text{M}$ (**CO**), $4.4 \pm 0.6 \mu\text{M}$ (**SAL**) and $4.2 \pm 0.2 \mu\text{M}$ (**COSAL**) while the concentration required to inhibit at 100 % the enzymatic reaction was 130 μM for **CO**, 20 μM for **SAL** and 10 μM for **COSAL**. The trends shown in Fig. 6 suggest different mechanisms involved in the reaction with the enzyme.

Molecular docking

Considering the ability of several LOX inhibitors of expressing their activity by targeting the catalytic binding site^{29,40–42}, we initially performed simulations considering our test compounds as competitive inhibitors. In order to validate the docking protocol chosen, we decided to dock at first the inhibitor 3,4-dihydroxybenzoic acid (dhb), obtained as oxidation product of quercetin by LOX-3²⁹, in its binding site. A satisfactory overlapping of the docked pose with the crystallized one was obtained, as showed in Fig. S16, with a RMSD of 0.6176 Å and a scoring function (expressed as binding affinity) of -5.5 kcal/mol . A closer view of intermolecular interactions between the docked pose of dhb and LOX residues (Fig. 7A) shows a series of

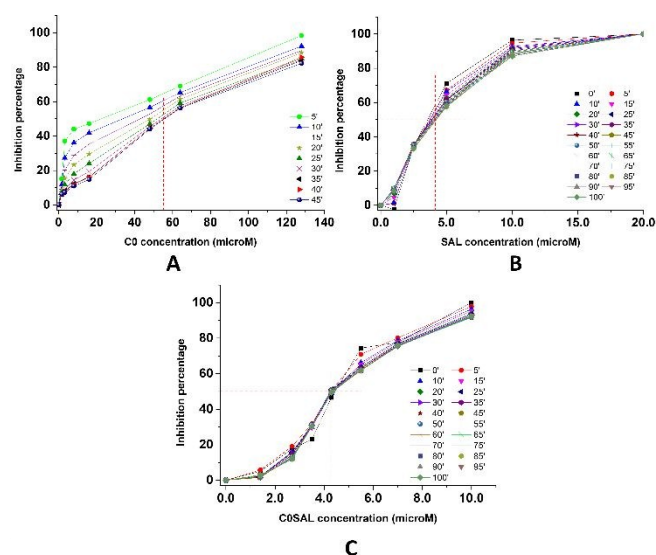


Fig. 6 Inhibition percentage observed at different concentration of **CO** (A), **SAL** (B) or **COSAL** (C) at different time after the mixing of the reactants; linoleic acid 32 μM , lipoxigenase 0.88 nM, pH 7.4 TRIS buffer, T 25°C.

π interactions, e.g. T-shaped with HIS518 and π -alkyl with LEU565 and ALA561. In the same way, the docking protocol was applied to $[\text{Cu}(\text{phen})_2(\text{H}_2\text{O})]^{2+}$, **SAL** and $[\text{Cu}(\text{phen})_2(\text{SAL})]^{2+}$, obtaining in each case high positive scoring functions (7.7, 38.5, 69.2 kcal/mol for **SAL**, $[\text{Cu}(\text{phen})_2(\text{H}_2\text{O})]^{2+}$ and $[\text{Cu}(\text{phen})_2(\text{SAL})]^{2+}$, respectively) due to hindering shape effects

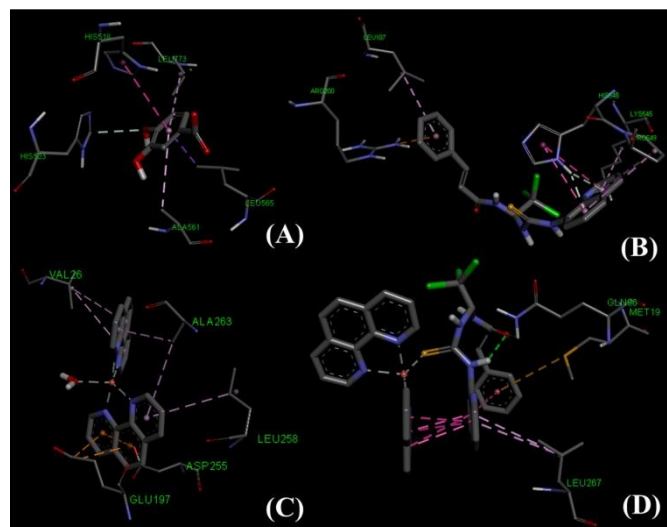


Fig. 7 docked poses of dhb (A), **SAL** (B), $[\text{Cu}(\text{phen})_2(\text{H}_2\text{O})]^{2+}$ (C), $[\text{Cu}(\text{phen})_2(\text{SAL})]^{2+}$ (D) and intermolecular interactions with surrounding residues of soybean LOX.

related to the bulky nature of the ligands. These results, in analogy with previous docking studies performed on similar Cu(II) mixed complexes^{39,43}, prompted us to explore the possibility that their inhibitory activity was a result of allostery. A cavity previously identified and located between the C-terminus and N-terminus domains of LOX-3 was chosen as potential binding site for the tested compounds. In this case, scoring functions of -9.6 , -8.9 and -8.1 kcal/mol were obtained for **SAL**, $[\text{Cu}(\text{phen})_2(\text{H}_2\text{O})]^{2+}$ and $[\text{Cu}(\text{phen})_2(\text{SAL})]^{2+}$, respectively. Full view and zoom of the binding cavities determined for the docked compounds are showed in Fig. 8 for $[\text{Cu}(\text{phen})_2(\text{SAL})]^{2+}$ and in Fig. S17 and S18 for $[\text{Cu}(\text{phen})_2(\text{H}_2\text{O})]^{2+}$ and **SAL**. Analysis of the docked pose for **SAL** (Fig. 7B) revealed several π interactions (e.g. π - π T-shaped with PRO549, π alkyl with LEU187 and LYS547). A closer inspection of the docked poses revealed for $[\text{Cu}(\text{phen})_2(\text{H}_2\text{O})]^{2+}$ (Fig. 7C) a series of hydrophobic interactions (mainly π -Alkyl, e.g. with VAL26, ALA263 and LEU258), while for $[\text{Cu}(\text{phen})_2(\text{SAL})]^{2+}$ (Fig. 7D), along with π interactions with MET19 and ARG786, we have in addition a hydrogen bond between N-H of GLN96 and carbonyl oxygen of **SAL** moiety. The docked pose of $[\text{Cu}(\text{phen})_2(\text{SAL})]^{2+}$ is further stabilized by several intramolecular non-covalent interactions, e.g. π - π stacking between quinoline fragment of **SAL** and one of the phenanthroline molecules, and a hydrogen bond between one of the thioamidic $-\text{NH}$ groups and carbonyl oxygen, both belonging to the **SAL** moiety.

ARTICLE

Biological mechanism

First, we were curious if there was any effect on cell ultrastructure induced by **SAL** alone. We employed A2780 and SKOV3 cells and performed transmission electron microscopy analysis. We revealed that cells treated by **SAL** have not suffered from any ultrastructural aberrations (Suppl. Fig. S19). In contrast, treatment by **C0** induced massive alterations of endoplasmic reticulum (ER) and partially also mitochondria.⁹ Then, to assess cytotoxic properties of newly synthesized **COSAL** compound, we performed viability assay based on activity of cellular NAD(P)H-dependent oxidoreductases (MTT assay). While the treatment by **SAL** had no significant effect in wide concentration range (Fig. S20A), we revealed massive reduction of cell viability when **SAL** was bound to **C0** (Fig. S20B). The cytotoxicity rate was similar to the treatment with individual **C0** or **C0** co-treated with **SAL** (Fig. S20C). EC₅₀ of **COSAL** on A2780 cells was (0.68 ± 0.05) μM, while those of **SAL** and **C0** were (56 ± 4) μM and (0.94 ± 0.04) μM, respectively. To reveal the possible mechanism of action of the **COSAL** complex, we first analyzed intracellular levels of phosphorylated histone γ-H2AX that recruits in DNA damage. After **COSAL** treatment on A2780 and SKOV3 cells, γ-H2AX was massively accumulated in A2780 cells, while the SKOV3 cells contained significant basal expression of γ-H2AX and the relative increase was minor (Fig 9A). We have recently described that **C0** complex and its derivatives induce cell death by activation of unfolded protein response. Similarly, treatment by **COSAL** induces expression of GRP-78 and DDIT3 regulators of ER-stress response in SKOV3 ovarian cancer cells, as can be seen in Fig. 9B. Moreover, to elucidate whether **COSAL** induced cell death via activation unfolded protein

response, the A2780 and SKOV3 ovarian cancer cells were treated either with **COSAL** alone or in combination with tauroursodeoxycholic acid. TUDCA reverted cytotoxic effect of **COSAL** in A2780 cells, and this effect was even more pronounced in SKOV3 cells (Fig. 10). This might suggest that induction of ER-stress is the preferred driving mechanism of cell death induced by **COSAL**.

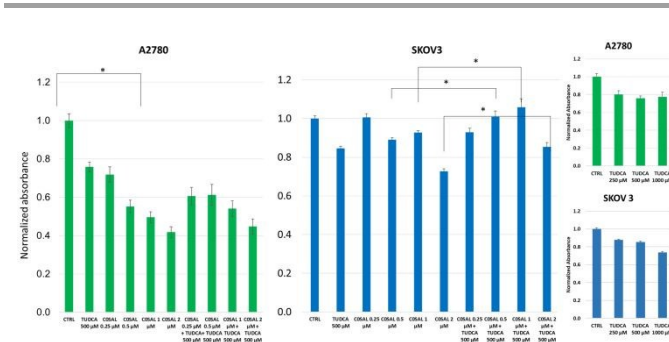


Fig. 10 SKOV3 and A2780 cells were cultured for 18 hrs either in presence or absence of **COSAL** and/or SKOV3 and A2780 cells were cultured for 18 hrs either in presence or absence of **COSAL** and/or tauroursodeoxycholic acid (TUDCA) at indicated concentrations. Then, the cell viability was determined by conversion of the 4-nitro blue tetrazolium chloride to formazan followed by measurement of OD at 570 nm (MTT assay). The plots represent means and SDs from three independent experiments performed in technical pentaplicates. Asterisks indicate statistical significance at $p < 0.05$

Conclusions

By reaction between $[\text{Cu}(\text{phen})_2(\text{H}_2\text{O})](\text{ClO}_4)_2$ (**C0**) and the ER stress modulator salubrinol the novel complex $[\text{Cu}(\text{phen})_2(\text{salubrinol})](\text{ClO}_4)_2$ (**COSAL**) was obtained. The stoichiometry and the complex formation constant of **COSAL** were determined by mass spectrometry and spectrophotometric measurements. The experimental results shown the metal ion coordinated by the thionic group of the salubrinol molecule, as confirmed also by the theoretical calculations. DPPH radical scavenging ability of the novel compound and of the precursors **C0** and **SAL** were studied, showing that the coordination with the $\text{Cu}(\text{phen})_2$ backbone increases the reducing activity of the salubrinol of the 260 % at 3 min. Studies on soybean lipoxygenase inhibition showed that the concentration of **COSAL** required to inhibit the 50 % of the enzyme was lower than that of **C0** (4.2 μM versus 55 μM) and comparable to that of salubrinol. However, the concentration required to inhibit at 100 % the enzymatic reaction was lower than those of **C0** or salubrinol (10 μM versus 130 μM or 20 μM). Docking calculations performed on the former enzyme suggest allosteric modulation as a possible mechanism of inhibition by the studied compounds. **COSAL** revealed to possess high potency in terms of cytotoxicity on A2780 cells, 82-fold higher than Salubrinol and 1.4-fold higher than **C0**. Treatment with **COSAL** in SKOV3 ovarian cancer cells induces expression of GRP-78 and DDIT3 regulators of ER-stress response. In the presence of TUDCA, the cytotoxic effect of **COSAL** was reverted, suggesting that the induction of ER-stress is indeed the driving mechanism of cell death caused by **COSAL**.

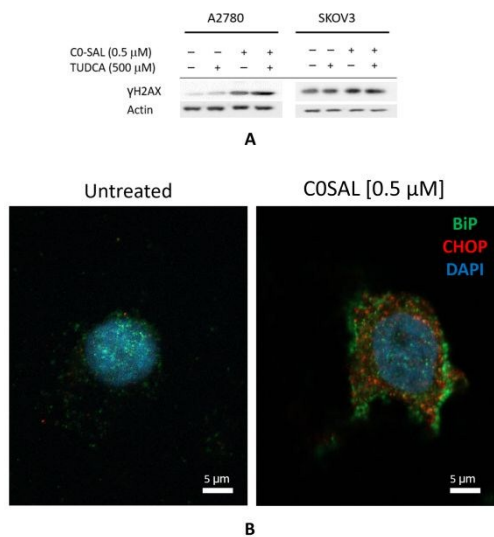


Fig. 9 (A) Intracellular levels of phosphorylated histone γ-H2AX after **COSAL** treatment on A2780 and SKOV3 cells; (B) expression of GRP-78 and DDIT3 regulators of ER-stress response in SKOV3 ovarian cancer cells treated with **COSAL**. SKOV3 cells were cultured for 18hrs in presence of **COSAL** and then analyzed by immunofluorescent microscopy for expression of GRP-78 (green) and DDIT3 proteins (red). Nuclei (blue) were visualized by DAPI staining.

In A2780 cells treated with COSAL γ -H2AX was accumulated, suggesting that also DNA damage was involved.

In conclusion, this research, being a cross-disciplinary study that involves metallobiochemistry, pharmacology, medicine, and toxicology, might provide a better understanding of the mechanisms of action of potential copper anticancer drugs and give useful insights for the design of new active species.

Conflicts of interest

"There are no conflicts to declare".

Acknowledgements

S. M. acknowledges MIUR for his PhD fellowship (XXXIV cycle). We acknowledge the CeSAR (Centro Servizi Ricerca d'Ateneo) core facility of the University of Cagliari and Dr. Sandrina Lampis for assistance with the generation of NMR data. We acknowledge the CeSAR (Centro Servizi d'Ateneo per la Ricerca) of the University of Cagliari, Italy, for the High Resolution Mass Spectrometry experiments performed with Orbitrap Elite, Thermo Fisher Scientific. L. M. is Brno PhD Talent Scholarship Holder – Funded by the Brno City Municipality. We acknowledge the core facility CELLIM of CEITEC supported by the Czech-Biolmaging large RI project (LM2018129 funded by MEYS CR) for their support with obtaining scientific data presented in this paper

Notes and references

- 1 F. Trudu, F. Amato, P. Vaňhara, T. Pivetta, E. M. Peña-Méndez and J. Havel, *J. Appl. Biomed.*, 2015, **13**, 79–103.
- 2 D. S. Sigman, D. R. Graham, V. D. Aurora, A. M. Stern and D. Aurora, *J. Biol. Chem.*, 1979, **254**, 12269–12272.
- 3 T. Pivetta, M. Dolores, F. Demartin, C. Castellano, S. Vascellari, G. Verani and F. Isaia, *J. Inorg. Biochem.*, 2011, **105**, 329–338.
- 4 T. Pivetta, F. Isaia, G. Verani, C. Cannas, L. Serra, C. Castellano, F. Demartin, F. Pilla, M. Manca and A. Pani, *J. Inorg. Biochem.*, 2012, **114**, 28–37.
- 5 T. Pivetta, V. Lallai, E. Valletta, F. Trudu, F. Isaia, D. Perra, E. Pinna and A. Pani, *J. Inorg. Biochem.*, 2015, **15**, 107–114.
- 6 E. Cadoni, E. Valletta, G. Caddeo, F. Isaia, M. G. Cabiddu, S. Vascellari and T. Pivetta, *J. Inorg. Biochem.*, 2017, **173**, 126–133.
- 7 T. Pivetta, F. Trudu, E. Valletta, F. Isaia, C. Castellano, F. Demartin, R. Tuveri, S. Vascellari and A. Pani, *J. Inorg. Biochem.*, 2014, **141**, 103–113.
- 8 S. Vascellari, E. Valletta, D. Perra, E. Pinna, A. Serra, F. Isaia, A. Pani and T. Pivetta, *RSC Adv.*, 2019, **9**, 5362–5376.
- 9 L. Morán, T. Pivetta, S. Masuri, K. Vašíčková, F. Walter, J. Prehn, M. Elkalaf, J. Trnka, J. Havel and P. Vaňhara, *Metallomics*, 2019, **11**, 1481–1489.
- 10 S. Wang and R. J. Kaufman, *J. Cell Biol.*, 2012, **197**, 857–867.
- 11 M. Kitamura, *Semin. Immunopathol.*, 2013, **35**, 259–275.
- 12 M. Boyce, K. F. Bryant, C. Jousse, K. Long, H. P. Harding, D. Scheuner, R. J. Kaufman, D. Ma, D. M. Coen, D. Ron and J. Yuan, *Science (80-.)*, 2005, **307**, 935–939.
- 13 K. Long, M. Boyce, H. Lin, J. Yuan and D. Ma, *Bioorg. Med. Chem. Lett.*, 2005, **15**, 3849–3852.
- 14 M. Strohalm, D. Kavan, P. Nova and M. Volny, *Anal. Chem.*, 2010, **82**, 4648–4651.
- 15 T. H. J. Niedermeyer and M. Strohalm, *PLoS One*, 2012, **7**, e44913. DOI: 10.1039/D0MT00006J
- 16 P. Gans, A. Sabatini and A. Vacca, *Talanta*, 1996, **43**, 1739–1753.
- 17 J. P., *Ann. Chim. Appl.*, 1928, **9**, 113–203.
- 18 J. S. Renny, L. L. Tomasevich, E. H. Tallmadge and D. B. Collum, *Angew. Chemie Int. Ed.*, 2013, **52**, 11998–12013.
- 19 J. Liu, K.-L. He, X. Li, R.-J. Li, C.-L. Liu, W. Zhong and S. Li, *Curr. Med. Chem.*, 2012, **19**, 6072–6079.
- 20 C. Tolia, A. N. Papadopoulos, C. P. Raptopoulou, V. Psycharis, C. Garino, L. Salassa and G. Psomas, *J. Inorg. Biochem.*, 2013, **123**, 53–65.
- 21 Z. Bousourani, G. D. Geromichalos, S. Katsamakas, V. Psycharis and C. P. Raptopoulou, *Mater. Sci. Eng. C*, 2019, **94**, 493–508.
- 22 F. Neese, *Wiley Interdiscip. Rev. Comput. Mol. Sci.*, 2012, **2**, 73–78.
- 23 M. D. Hanwell, D. E. Curtis, D. C. Lonie, T. Vandermeersch, E. Zurek and G. R. Hutchison, *J. Cheminform.*, 2012, **4**, 17.
- 24 C. Adamo and V. Barone, *J. Chem. Phys.*, 1999, **110**, 6158–6170.
- 25 F. Weigend and R. Ahlrichs, *Phys. Chem. Chem. Phys.*, 2005, **7**, 3297–3305.
- 26 T. Y. Nikolaienko, L. A. Bulavin and D. M. Hovorun, *Comput. Theor. Chem.*, 2014, **1050**, 15–22.
- 27 Chemcraft - graphical software for visualization of quantum chemistry computations. <https://www.chemcraftprog.com>.
- 28 O. Trott and A. J. Olson, *J. Comput. Chem.*, 2009, 455–461.
- 29 O. Y. Borbulevych, J. Jankun, S. H. Selman and E. Skrzypczak-Jankun, *Proteins Struct. Funct. Bioinforma.*, 2003, **54**, 13–19.
- 30 G. M. Morris, H. Ruth, W. Lindstrom, M. F. Sanner, R. K. Belew, D. S. Goodsell and A. J. Olson, *J. Comput. Chem.*, 2009, **30**, 2785–2791.
- 31 Dassault Systèmes BIOVIA, Discovery Studio Viewer, v19, San Diego: Dassault Systèmes, 2019.
- 32 C. Hao and R. E. March, *J. Mass Spectrom.*, 2001, **36**, 509–521.
- 33 J. Foley, D. Kenefick, D. Phelan, S. Tyagi and B. Hathaway, *J. Chem. Soc., Dalt. Trans.*, 1983, 2333–2338.
- 34 T. Pivetta, M. D. Cannas, F. Demartin, C. Castellano, S. Vascellari, G. Verani and F. Isaia, *J. Inorg. Biochem.*, 2011, **105**, 329–338.
- 35 M. B. Ferrari, G. G. Fava and A. Montenero, *Cryst. Struct. Commun.*, 1975, **4**, 577.
- 36 G. Murphy, C. Murphy, B. Murphy and B. Hathaway, *J. Chem. Soc. Dalt. Trans.*, 1997, **2**, 2653–2660.
- 37 A. W. Addison, T. N. Rao, J. Reedijk, J. van Rijn and G. C. Verschoor, *J. Chem. Soc., Dalt. Trans.*, 1984, 1349–1356.
- 38 D. Huang, B. Ou and R. L. Prior, *J. Agric. Food Chem.*, 2005, **53**, 1841–1856.
- 39 Z. Bousourani, G. D. Geromichalos, S. Katsamakas, V. Psycharis, C. P. Raptopoulou, D. Hadjipavlou-Litina, D. Sahpazidou and C. Dendrinou-Samara, *Mater. Sci. Eng. C*, 2019, **94**, 493–508.
- 40 E. Skrzypczak-Jankun, K. Zhou, N. McCabe, S. Selman and J. Jankun, *Int. J. Mol. Med.*, 2003, 17–24.
- 41 E. Skrzypczak-Jankun, K. Zhou and J. Jankun, *Int. J. Mol. Med.*, 2003, 415–420.
- 42 E. Skrzypczak-Jankun, O. Y. Borbulevych and J. Jankun, *Acta Crystallogr. Sect. D Biol. Crystallogr.*, 2004, **60**, 613–615.
- 43 Z. Bousourani, S. Katsamakas, G. D. Geromichalos, V. Psycharis, C. P. Raptopoulou, D. Hadjipavlou-Litina, E. Yiannaki and C. Dendrinou-Samara, *Mater. Sci. Eng. C*, 2017, **76**, 1026–1040.